The Use of *CloudSat* Data to Evaluate Retrievals of Total Ice Content in Precipitating Cloud Systems from Ground-Based Operational Radar Measurements

SERGEY Y. MATROSOV

Cooperative Institute for Research in Environmental Sciences, University of Colorado, and NOAA/Earth System Research Laboratory, Boulder, Colorado

(Manuscript received 16 January 2015, in final form 4 May 2015)

ABSTRACT

An approach is described to retrieve the total amount of ice in a vertical atmospheric column in precipitating clouds observed by the operational Weather Surveillance Radar-1988 Doppler (WSR-88D) systems. This amount expressed as ice water path (IWP) is retrieved using measurements obtained during standard WSR-88D scanning procedures performed when observing precipitation. WSR-88D-based IWP estimates are evaluated using dedicated cloud microphysical retrievals available from the *CloudSat* and auxiliary spaceborne measurements. The evaluation is performed using measurements obtained in extensive predominantly stratiform precipitation systems containing both ice hydrometeors aloft and rain near the ground. The analysis is based on retrievals of IWP from satellite and the ground-based KWGX and KSHV WSR-88D that are closely collocated in time and space. The comparison results indicate a relatively high correlation between satellite and WSR-88D IWP retrievals, with corresponding correlation coefficients of around 0.7. The mean relative differences between spaceborne and ground-based estimates are around 50%–60%, which is on the order of IWP retrieval uncertainties and is comparable to the differences among various operational *CloudSat* IWP products. The analysis performed in this study suggests that the quantitative information on ice content of precipitation systems can generally be obtained from operational WSR-88D measurements, when they perform routine scans to observe precipitation. The limitations of WSR-88D IWP estimates due to radar beam tilt restrictions and the overshooting effects due to Earth's sphericity are discussed.

1. Introduction

With a few gaps in the western United States, the Next Generation Weather Radar (NEXRAD) network of S-band (~3 GHz) Weather Surveillance Radar-1988 Doppler (WSR-88D) units covers most of the area in the lower 48 states. Although these units can detect even some nonprecipitating clouds (Melnikov et al. 2011), the main objective of the NEXRAD network is to provide data for quantitative precipitation estimation (QPE) and information about storm movements and hazardous weather. The WSR-88D-based precipitation retrievals are the core part of the National Mosaic and Multi-Sensor QPE (NMQ) system (Zhang et al. 2011). The dual-polarization upgrade of NEXRAD conducted in 2012–13 further enhances WSR-88D rainfall retrievals (e.g., Ryzhkov et al. 2005) and provides a means for precipitating hydrometeor identification in such classes as rain, hail, graupel, and wet/dry snow (e.g., Bringi and Chandrasekar 2001).

WSR-88D operations during precipitation events are conducted in repetitive scan sequences, which are determined by the volume coverage patterns (VCPs). Each VCP consists of several azimuthal scans at selected radar beam elevation angles (tilts). The VCPs used for precipitation observations typically include 9–14 such scans at different tilts. The lowest and the highest tilts correspond to the 0.5° and 19.5° center beam elevations, respectively. A total VCP sequence takes approximately 5 min.

Although the lower tilt WSR-88D data are most informative about precipitation near the ground, the combination of measurements from all tilts can be used to obtain information about the whole vertical extent of observed precipitation systems including ice regions of such systems as will be shown in section 4. Often when the lowest available unblocked beam measurements are coming from

Corresponding author address: Sergey Y. Matrosov, R/PSD2, 325 Broadway, Boulder, CO 80305.
E-mail: sergey.matrosov@noaa.gov

DOI: 10.1175/JAMC-D-15-0032.1

the heights above the layer of liquid precipitation, approaches that involve the vertical profile of reflectivity are used to relate these measurements aloft to the ones near the ground (e.g., Kirstetter et al. 2013). Although radar reflectivity data from ice regions above freezing levels can be used to infer quantitative information about ice contents (e.g., Matrosov 1997), such information is not currently retrieved from operational WSR-88D measurements.

The ice content information from higher parts of precipitating systems that are producing rain is important since ice melting is a dominant rainfall formation process in stratiform precipitation (e.g., Bringi and Chandrasekar 2001). Even in tropics about 40% of rain is stratiform-like (Houze 1997). In midlatitudes often more than half of total liquid precipitation comes from stratiform-like systems (e.g., Matrosov et al. 2014). Such systems are considered in this study.

The quantitative information on clouds is often obtained using satellite measurements. The use of passive satellite techniques for inferring ice content in cloud systems resulting in rain near the ground is, however, impeded by the fact that ice and water hydrometeors both contribute to the combined radiometric signal and their independent retrievals are not straightforward. On the other hand, the nadir-pointing W-band (~94 GHz) cloud-profiling radar (CPR) on board the *CloudSat* satellite (e.g., Stephens et al. 2008) is able to provide ice contents of precipitating systems in presence of different water phases in the same vertical column because of the nature of vertically resolved measurements.

The objective of this study was to assess the ability of WSR-88D units to provide quantitative information on ice contents in clouds, which are observed as part of precipitating systems producing rain. This assessment is achieved by comparing WSR-88D-based estimates with closely collocated in space and time *CloudSat*-based retrievals. Combined cloud and rain retrievals from ground-based radars will potentially allow for studying precipitation formation processes in more detail, thus the availability of such retrievals from scanning radar measurements could enhance the utility of routine WSR-88D observations. The ice cloud remote sensing is one of the principal strengths of the *CloudSat* project, so comparing WSR-88D ice cloud parameter estimates with *CloudSat* retrievals could be considered an important step in evaluating the use of scanning weather radar measurements for cloud-property retrievals.

2. Datasets and parameters used for comparisons of WSR-88D and *CloudSat* retrievals

The WSR-88D level-II data available to the users are sampled utilizing a grid with resolution of 1 km along the radar beam by 1° azimuth in the legacy NEXRAD resolution mode and using a 0.25 km × 0.5° grid in the super-resolution mode, which implies oversampling. The super-resolution mode has been in use approximately since the summer of 2008. However, since the WSR-88D angular beamwidth is approximately 1° (one-/two-way at 3/6-dB level), beam broadening degrades the actual spatial resolution of NEXRAD units as the range of observations increases. For normal atmospheric conditions Fig. 1 schematically shows the WSR-88D vertical resolution for 10-, 50-, 100-, 150-, and 200-km radar distances and 14 characteristic elevation angles, which are employed in different precipitation VCPs. For better visualization, the actual along-beam resolution is exaggerated and the resolution volumes for a given distance at different elevation angles are slightly shifted with respect to each other.

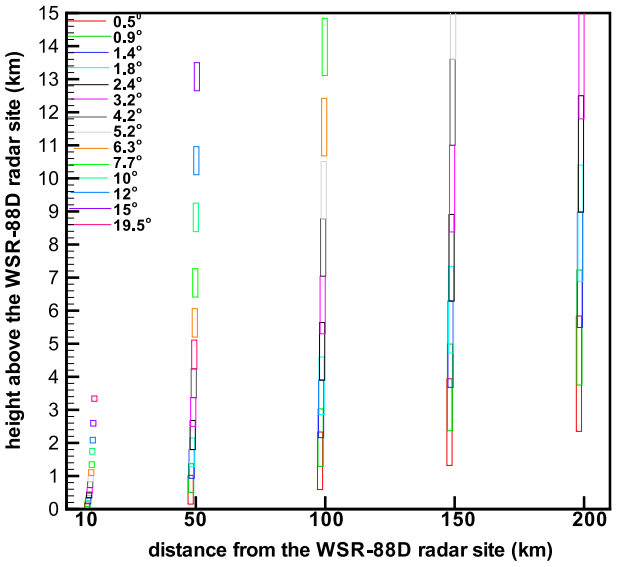

FIG. 1. A schematic depiction of the WSR-88D resolution volumes (assuming a 1.8-km range averaging and normal atmospheric conditions) at 14 different radar center beam elevation angles for distances of 10, 50, 100, 150, and 200 km. For better visualization the resolution volumes for a given distance are slightly shifted relative to each other.

It can be seen from Fig. 1 that depending on the distance from the radar there could be overlapping or gaps in the WSR-88D vertical coverage. There are also bounds on the maximal sampling height because of the 19.5° elevation angle limit of the antenna tilt, which is most pronounced for shorter horizontal distances, and also on the minimal sampling height, which is most pronounced at longer distances because of Earth's sphericity effects. For data in Fig. 1, these effects were accounted for using approaches described in (Doviak and Zrnic 1993, their section 2.2.3). It should also be noted that actual overlapping/gap features may differ

somewhat from the ones depicted in Fig. 1 when elevation angles for particular VCPs chosen by the radar operators are slightly different from the ones used in this figure and also if VCPs with smaller numbers of elevation scans are used for observations or atmospheric conditions deviate from normal.

The *CloudSat* CPR resolution volume is about 1.5 km across the satellite track, approximately 1.8 km along the track, and 0.5 km in the vertical direction (Tanelli et al. 2008). Vertical oversampling allows for providing vertical profiles of observed CPR reflectivity factor with an increment of 0.24 km. Overall the CPR and WSR-88D along-beam spatial resolutions are not vastly different, which is favorable for retrieval intercomparisons. The actual vertical resolutions, however, could be quite different (see Fig. 1) depending on the distance of the WSR-88D resolution volume from a ground-based radar site.

While a relatively poor and distance-dependent cross-beam WSR-88D resolution hampers retrievals of vertical profiles of ice cloud parameters from operational NEXRAD measurements, these measurements can be potentially used for estimating important integrated cloud properties such as ice water path (IWP), which represents the vertically integrated ice water content (IWC) in an atmospheric column. IWP is an important ice cloud parameter that is routinely retrieved from *CloudSat* measurements. This study further focuses on quantitative evaluations of prospects for WSR-88D-based IWP retrievals in precipitating ice regions that are part of stratiform systems, which produce rain and are observed by operational NEXRAD units.

3. Choice of observational events and *CloudSat* IWP products

Comparisons of WSR-88D and CPR-based retrievals of IWP in precipitating cloud systems are most practical for the observations conducted when the *CloudSat* satellite passes over the vicinity of the NEXRAD sites. Such overpasses during spatially extensive precipitation events, however, are not very common. This study further focuses on 12 mostly stratiform precipitation events, which occurred during *CloudSat* crossings over the vicinity of two WSR-88D units: namely the KGWX Greenwood Springs, Mississippi, radar (33.8969°N, 88.3292°W) and the KSHV Shreveport, Louisiana, radar (32.4508°N, 93.8414°W). These overpasses occurred during the period 2006–12. The WSR-88D and CPR measurements obtained during these overpasses were previously used to compare *CloudSat* rain-rate retrievals over land utilizing the reflectivity gradient method (Matrosov 2007) with estimates from standard NEXRAD approaches.

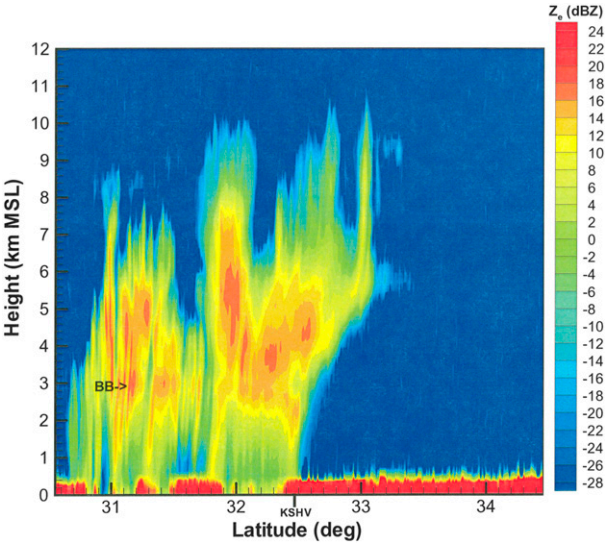

FIG. 2. A cross section of CPR reflectivity measurements during a *CloudSat* overpass above the KSHV WSR-88D site at 0820 UTC 15 Nov 2010. The vicinity of the KSHV location is shown on the *x* axis.

The dates of these mainly stratiform precipitation events are 13 September 2007, 16 July 2009, 1 August 2009, 4 October 2009, 16 May 2010, and 9 August 2012 for combined *CloudSat* and WSR-88D observations near the KGWX radar site, and 19 October 2006, 7 January 2007, 30 March 2008, 27 October 2009, 10 July 2010, and 15 November 2010 for the events in the vicinity of the KSHV radar site (Matrosov 2014). The *CloudSat* overpasses near the KGWX radar occur during the day time (1915 UTC) on the ascending satellite node, and crossings near the KSHV radar occur during the local nighttime (0820 UTC) on the descending satellite node.

Figure 2 shows the CPR W-band reflectivity factor Z_{ew} (hereafter, just reflectivity) measurements during one of the events when *CloudSat* passed over the vicinity of the KSHV site on 15 November 2010. Even though there are some localized areas of likely convection (e.g., between latitudes of 30.9° and 31°), from a radar perspective this is an event of mostly stratiform precipitation, which is characterized by a radar ''bright band'' (BB; Bringi and Chandrasekar 2001). The BB, which is located just below the freezing level (i.e., the 0°C isotherm), is usually several hundred meters thick and separates predominantly ice regions of precipitation systems above and the liquid hydrometer layer containing rain below. Although the BB radar signals at W band are strongly influenced by the signal attenuation in mixed phase (e.g., Sassen et al. 2007; Matrosov 2008), its appearance as viewed by down-looking radars is similar

to BBs usually observed at nonattenuated and weakly attenuated radar frequencies when reflectivity enhancements caused by ice/snow melting particles and changes in hydrometeor fall speeds result in the bright band. The ice hydrometeor regions observed in precipitating systems above the BB are of the main interest to this study.

Several IWP retrieval products are available from the *CloudSat* Data Processing Center (DPC). The IWP estimates from the level-2B radar-only cloud water content product (2B-CWC-RO) are available for all CPR profile measurements (Austin et al. 2009). CPR reflectivity data are used to derive cloud parameters in this product utilizing a spherical particle model. IWP data are also available from the level-2B radar-visible optical depth cloud water content product (2B-CWC-RVOD) developed by the same authors. In addition to the CPR data, 2B-CWC-RVOD retrievals use collocated optical depth data from the Moderate Resolution Imaging Spectroradiometer (MODIS) flown on board the *Aqua* satellite, which, as *CloudSat*, is part of the A-Train satellite formation. Since the optical thickness data are not always available, the 2B-CWC-RVOD IWP estimates are not provided for all CPR profiles.

The *CloudSat* DPC also distributes the level-2C ice-cloud-property product (2C-ICE; Deng et al. 2013), which contains IWP data. Generally 2C-ICE product retrievals use *CloudSat* CPR and collocated lidar data from the *CALIPSO* satellite, which also is part of the A-Train. When lidar data are unavailable because of the total extinction of *CALIPSO* signals in optically thick clouds (which is very often the case with the ice regions of precipitating systems resulting in rain), the 2C-ICE IWC retrievals can use empirical relationships based on the W-band radar reflectivity and temperature data.

In precipitating ice layers *CloudSat* CPR measurements are affected by multiple scattering (MS), which increases observed reflectivities compared to their intrinsic values. The reflectivity increase caused by MS, however, is counteracted by signal attenuation. The MS and attenuation effects partially balance each other, so their overall influence on CPR measurements is expected to be rather small (Matrosov and Battaglia 2009) and is often neglected.

In addition to the IWP products generally available from the *CloudSat* DPC, IWP estimates from the W-band radar reflectivity-only method, which was specifically developed for optically thick clouds composed of nonspherical ice particles (Matrosov and Heymsfield 2008, hereinafter MH08), were used in this study. Their relation for IWC,

$$\mathrm{IWC}(\mathrm{g\,m^{-3}}) \approx 0.086 Z_{ew}^{0.92} \quad (\mathrm{mm^6\,m^{-3}}), \qquad (1)$$

was applied to the CPR measurements for the events in this study. IWC values retrieved for a particular profile were then vertically integrated for cloud layers above the freezing level to obtain IWP. The temperature dependence of W-band IWC–Z_e relations for ice regions with $Z_{ew} > 0\,\mathrm{dB}Z$, which often dominate IWP of precipitating clouds (MH08), is not very pronounced and was neglected here. Note also that for such reflectivities, the IWC values from the relation (1) are rather close to the ones obtained using the self-similar Rayleigh–Gans approximation by Hogan and Westbrook (2014, their Fig. 5) developed for more complicated ice particle models.

4. The 15 November 2010 event case study

a. *Reconstruction of reflectivity vertical cross section data using WSR-88D data*

The event of 15 November 2010 observed during a *CloudSat* overpass over the vicinity of the KSHV radar is a typical one representing all 12 observational events mentioned in the previous section. For the time of the satellite overpass depicted in Fig. 2, Fig. 3 shows the WSR-88D map of the lowest beam tilt (i.e., a 0.49° center beam elevation angle) S-band reflectivities Z_{es} as obtained from the NEXRAD level-II products. The *CloudSat* ground track (shown by the white line) passed within 6 km from the KSHV radar site.

For the time of the *CloudSat* overpass, rainfall associated with this precipitating cloud system generally was observed to the south from the KSHV radar site and had typical S-band reflectivity values greater than about 20 dBZ (Fig. 3). The weak echo to the north of the radar site (~0–5 dBZ) is likely caused by biological targets, nonprecipitating hydrometeors and/or Bragg scattering. The thick high-altitude cloud anvil, which is seen in the CPR data just to the north of the ground-based radar (Fig. 2), is not observed with the lowest tilt NEXRAD measurements. The use of all tilt data collected during a WSR-88D volume scan, however, allows for reconstruction of the S-band reflectivity time–height cross section, which closely matches the CPR data in space and time. Figure 4 shows such a cross section along the *CloudSat* ground track reconstructed from the KSHV volume scan measurements taken around 0819 UTC.

During the KSHV cross-section reconstruction, which approximately corresponds to a virtual range–height indicator (RHI) scan, the WSR-88D reflectivities were averaged in 1.8-km range intervals to closely match the CPR horizontal resolution along the satellite track. The exact geographical coordinates for each CPR profile center were used for reconstructed KSHV profiles. To obtain reflectivity values in the reconstructed profile, the

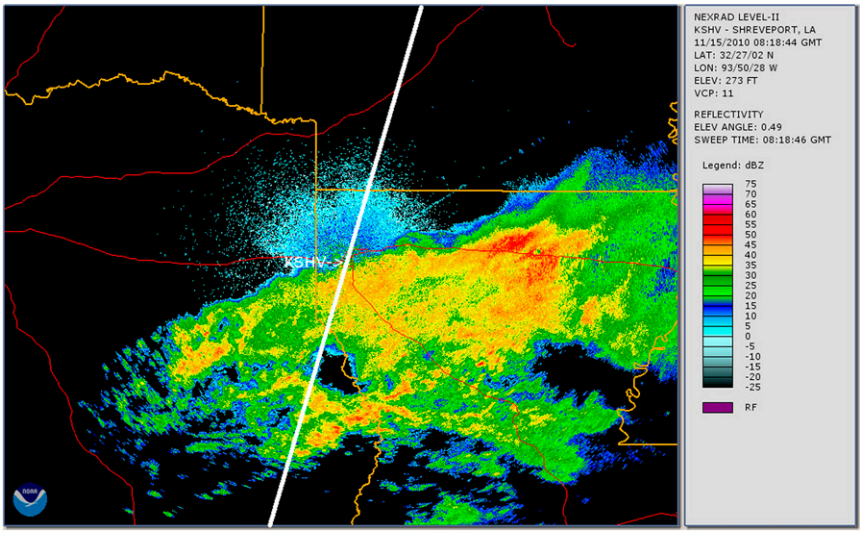

FIG. 3. Lowest tilt (0.49°) KSHV reflectivity data obtained during the *CloudSat* crossing approximately above the radar site at 0819 UTC 15 Nov 2010. The white line shows the CPR ground track.

linear interpolation in $mm^6 m^{-3}$ units between NEXRAD level-II reflectivity data from two neighboring ground radar beam azimuths, which bracket the direction to a CPR profile, was used. The actual beam elevation tilts for the 0819 UTC KSHV volume scan were 0.49°, 1.44°, 2.4°, 3.4°, 4.3°, 5.3°, 6.2°, 7.5°, 8.7°, 10.1°, 12.0°, 14.0°, 16.7°, and 19.5° (VCP-11). This VCP does not have the 0.9° tilt, which is present, for example, in VCP-12 used for some other events considered in this study, but allows for somewhat better coverage for higher beam tilts (>10°) than other precipitation VCPs. The 19.5° WSR-88D tilt limit does not allow for WSR-88D sensing the regions above the radar site (a so-called cone of silence in Fig. 4). Earth's sphericity results in the data absence in the layer near the ground, whose thickness increases with range from the ground-based radar site.

From comparing closely matched WSR-88D and *CloudSat* reflectivity cross sections in Figs. 2 and 4, one can see that, because of the relatively high sensitivity of WSR-88D reflectivity measurements [from approximately −20 to −25 dBZ at 10 km for typical scan rates (Melnikov et al. 2011)], the ground-based radar is able to resolve main features in the precipitating ice cloud regions seen in very sensitive (the lowest detectable CPR reflectivity is about −29 dBZ) satellite observations. One exception is the low reflectivity regions near cloud tops. These regions with reflectivities less than 0 dBZ, however, are not expected to significantly contribute to IWP of typical stratiform precipitating systems (MH08). A poorer vertical resolution of WSR-88D measurements (as compared to the CPR resolution) prevents observing the fine cloud structure revealed by the CPR. This fact indicates that a primary utility of operational WSR-88D measurements for precipitating cloud quantitative estimates is likely be in retrieving columnar IWP rather than in inferring ice water content profiles with a good vertical resolution. It is also worth mentioning that, for a given cloud volume of hydrometeors oriented preferably with major dimensions in the horizontal plane, WSR-88D horizontal polarization reflectivities used in this study (unlike vertical polarization reflectivities) are not expected

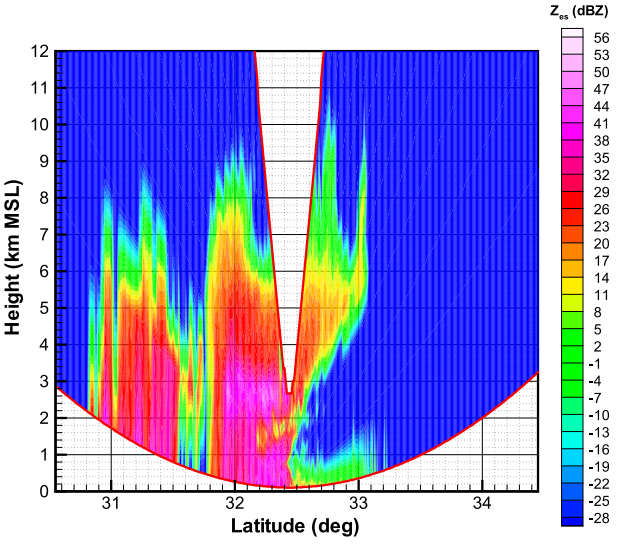

FIG. 4. A reconstructed vertical cross section of KSHV reflectivities at 0820 UTC 15 Nov 2010 in a plane of the *CloudSat* overpass from Fig. 2. Red border lines in the image correspond to the lower/higher edges of the lowest/highest WSR-88D tilts (i.e., 0.0° and 20.0°, respectively).

to exhibit significant dependence on the direction of viewing.

b. *Estimating IWP using WSR-88D measurements*

A vertical integration of IWC values is needed to calculate IWP. As for conventional nonpolarimetric WSR-88D QPE retrievals, estimations of cloud ice content using radar-only data are typically based on radar reflectivity measurements. During the collocated precipitation events, which are considered here, available level-II WSR-88D variables included short-range reflectivities for distances less than 230 km. Operational WSR-88D measurements starting from 2013 additionally provide polarimetric radar variables (e.g., differential reflectivity, differential phase shift, and the copolar correlation coefficient). However, because polarimetric data were not available for the events considered here anyway, the relatively well-established reflectivity-based ice content retrievals were used here. Such retrievals remain a viable approach for IWP estimates from radar measurements.

Hogan et al. (2006) provided a relation for IWC retrievals based on S-band radar reflectivity Z_{es} and temperature t. This relation was further used in this study for ice content estimates from the WSR-88D measurements:

$$\log_{10}\mathrm{IWC}\ (\mathrm{g\,m^{-3}}) = 0.06Z_{es}\ (\mathrm{dB}Z) - 0.02t\ (^{\circ}\mathrm{C}) - 1.7. \tag{2}$$

According to these authors, the temperature dependence of S-band IWC–Z_e relations at higher reflectivities is significantly stronger than that for W band. At S-band frequencies ice hydrometeor sizes are generally in the Rayleigh scattering regime and the particle shape dependence of backscatter is not as pronounced as at millimeter-wavelength radar frequencies.

The reconstructed cross section of KSHV reflectivities matching the *CloudSat* reflectivity cross section was used to calculate IWP values from WSR-88D data corresponding to each CPR profile. Measurements at an ith elevation tilt provide an estimate of the ice water path amount, IWP_i, contained in a layer between the upper $[h_i^{(u)}]$ and lower $[h_i^{(l)}]$ beam edges of this tilt:

$$\mathrm{IWP}_i = \mathrm{IWC}_i[h_i^{(u)} - h_i^{(l)}] \quad \text{if} \quad h_i^{(l)} > h_{\mathrm{fl}}, \tag{3a}$$

$$\mathrm{IWP}_i = \mathrm{IWC}_i[h_i^{(u)} - h_{\mathrm{fl}}] \quad \text{if} \quad h_i^{(l)} \le h_{\mathrm{fl}} \le h_i^{(u)}, \quad \text{and} \tag{3b}$$

$$\mathrm{IWP}_i = 0 \quad \text{if} \quad h_i^{(u)} < h_{\mathrm{fl}}, \tag{3c}$$

where h_{fl} is the freezing-level height and IWC_i is calculated based on the reflectivity data for this tilt and an average temperature in the layer between the beam edges $h_i^{(u)}$ and $h_i^{(l)}$. The beam edge height conditions in approximations (3) mostly exclude rain and BB contributions, although some minor BB influence may still exist in (3b) because of reflectivity enhancement. The beam edge heights are calculated assuming a 1° (3 dB one-way) beamwidth.

The total IWP value for a given profile was calculated by summing up IWP_i values for individual elevation tilts of a particular VCP with two adjustments. The first adjustment for IWP values accounts for overlapping beams in the event when the upper edge of the WSR-88D beam for a tilt i is higher than the lower edge of the beam for a higher tilt $i + 1$ (e.g., overlapping the VCP-12 tilts 2 and 3, corresponding to 0.9° and 1.3°, respectively). As a result of this adjustment, a nonnegative amount of $0.5(\mathrm{IWC}_i + \mathrm{IWC}_{i+1})[h_i^{(u)} - h_{i+1}^{(l)}]$ was subtracted from the total IWP.

The second adjustment accounts for undersampling (i.e., gaps) at the height intervals located between the upper and lower edges of two consecutive beams [i.e., when $h_i^{(u)} < h_{i+1}^{(l)}$]. Such undersampling, for example, occurs starting with the seventh VCP-11 tilt. In this case, a nonnegative amount of $0.5(\mathrm{IWC}_i + \mathrm{IWC}_{i+1})[h_{i+1}^{(l)} - h_i^{(u)}]$ was added to the total IWP value. Potential beamfilling issues [e.g., occurring when cloud is only partially present between heights $h_i^{(u)}$ and $h_i^{(l)}$] are not expected to significantly affect IWP_i values since effects of overestimating the cloud-layer thickness are mitigated by decreased estimates of this layer IWC_i values.

Since freezing-level heights are not readily available with acceptable accuracy from conventional WSR-88D data (especially because of the low vertical resolution of WSR-88D data at longer ranges) and IWP retrievals using these data should generally be possible operationally without concurrent *CloudSat* estimates of the BB heights, the information on temperature profiles (and hence on h_{fl}) needed for retrieving WSR-88D-based estimates IWP was taken from the European Centre for Medium-Range Weather Forecasts model data, which are usually available. Concurrent model data on freezing-level heights are also generally available with the operational NMQ system (e.g., Zhang et al. 2011) and could be used in an operational version of the IWP retrieval.

c. *Intercomparisons of WSR-88D and* CloudSat *IWP values*

For the 15 November 2010 observational case, WSR-88D-based IWP estimates obtained according to the procedure described above are depicted in Fig. 5. The vertical dashed lines indicate the boundaries of the "cone of silence," where NEXRAD IWP estimates either are not available or are diminished because of the maximum tilt limitation. MH08, 2B-CWC-RO, and 2C-ICE IWP

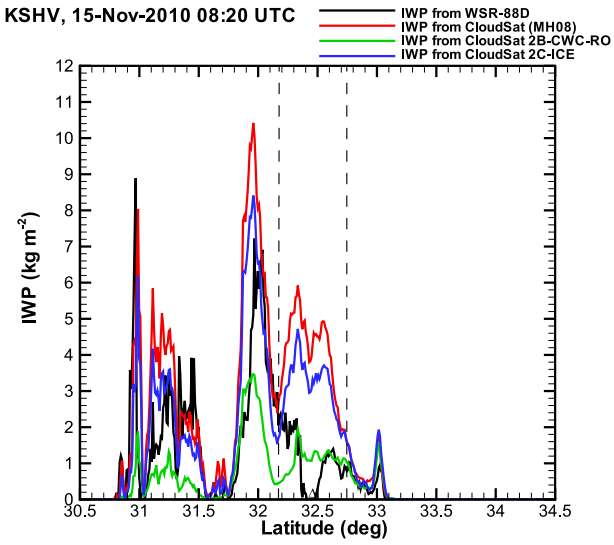

FIG. 5. KSHV and *CloudSat* IWP retrievals along the satellite ground track on 15 Nov 2010. The vertical dashed lines represent the boundaries of the cone of silence where WSR-88D measurements are absent or not available for whole vertical extent of the observed precipitation system.

estimates from *CloudSat* are also shown in this figure. 2B-CWC-RVOD IWP values differ from 2B-CWC-RO IWP values by only few percentage points and are not depicted. The negligible difference between IWC values corresponding to these products was also noted by Protat et al. (2010) who analyzed a large set of retrievals near Darwin, Australia. It can be seen from the presented data that outside the cone of silence there is an overall good correspondence between locations of IWP maxima and minima from the ground-based retrievals and all *CloudSat* products. For this event, IWP values change from the maximum values of about $10\,\mathrm{kg\,m^{-2}}$ to very small values near the latitude of 31.6°. The 2B-CWC-RO product provide the smallest IWP values from all the retrievals considered here.

5. Statistical characteristics of IWP comparisons

a. Intercomparisons of CloudSat *IWP retrievals*

For all 12 mostly stratiform precipitation events observed by the KGWX and KSHV radars during the *CloudSat* overpasses and listed in section 3, Fig. 6 shows the scatterplots among different *CloudSat*-based estimates of IWP. All these observational events were associated with rain in the lower layers of precipitating systems. This rain was predominantly of the stratiform type exhibiting radar BB features, though some isolated convection activity was also present. Mean rain rates for these events were approximately 2–2.5 $\mathrm{mm\,h^{-1}}$ reaching maximum values of around 15–20 $\mathrm{mm\,h^{-1}}$ in the convective regions (Matrosov 2014).

To assess the retrieval data in a quantitative sense, the correlation coefficient r between different IWP estimates as well as different statistical parameters characterizing the comparisons was calculated. These parameters include the normalized relative mean bias (RMB),

$$\mathrm{RMB} = \langle(\mathrm{IWP}_y - \mathrm{IWP}_x)\rangle\langle\mathrm{IWP}_x\rangle^{-1}100\%, \quad (4)$$

and the normalized mean absolute difference (NMAD),

$$\mathrm{NMAD} = \langle|\mathrm{IWP}_y - \mathrm{IWP}_x|\rangle\langle\mathrm{IWP}_x\rangle^{-1}100\%, \quad (5)$$

where the angle brackets denote averaging with respect to the whole dataset, and IWP_y and IWP_x denote IWP estimates plotted along y and x axes in Fig. 6, respectively. The statistical metrics characterizing *CloudSat* IWP comparisons are listed in Table 1. Note that 2C-ICE and 2B-CWC-RVOD IWP estimates are not available for some observed CPR profiles, which results in different numbers of compared data points for different comparing pairs.

As seen from Fig. 6 and Table 1, there is a high correlation among different *CloudSat* IWP retrievals. The highest correlation coefficient (0.98) is between MH08 and 2C-ICE IWP estimates. The relative bias and absolute difference between these two estimates are relatively small. While being very close to each other, the IWP estimates from the standard *CloudSat* 2B-CWC-RO and 2B-CWC-RVOD products are more than 50% lower on average than those obtained from the MH08 method and the 2C-ICE product. The underestimation of the IWP estimates from these standard *CloudSat* products relative to the 2C-ICE and MH08 retrievals is more distinct for higher values of the total columnar ice content (i.e., for $\mathrm{IWP} \gtrsim 1\,\mathrm{kg\,m^{-2}}$, see Figs. 6a,b,d), while the spread among different *CloudSat*-based IWP retrievals for smaller IWP values is generally smaller.

Although other ice cloud parameter retrievals that use *CloudSat* data, like the ones from the radar–lidar (DARDAR) method (Delanoe et al. 2013), exist, they were not used for comparisons in Fig. 6 because the retrievals from this method are not available from the *CloudSat* DPC. Note, however, that Deng et al. (2013) found that 2C-ICE and DARDAR ice cloud retrieval products (e.g., IWC and particle effective radii) were typically in general agreement.

Although intercomparisons of IWP values from different *CloudSat*-based techniques were not directly performed in previous studies, there are available intercomparisons of *CloudSat*-based IWC retrievals conducted during particular field campaigns. These

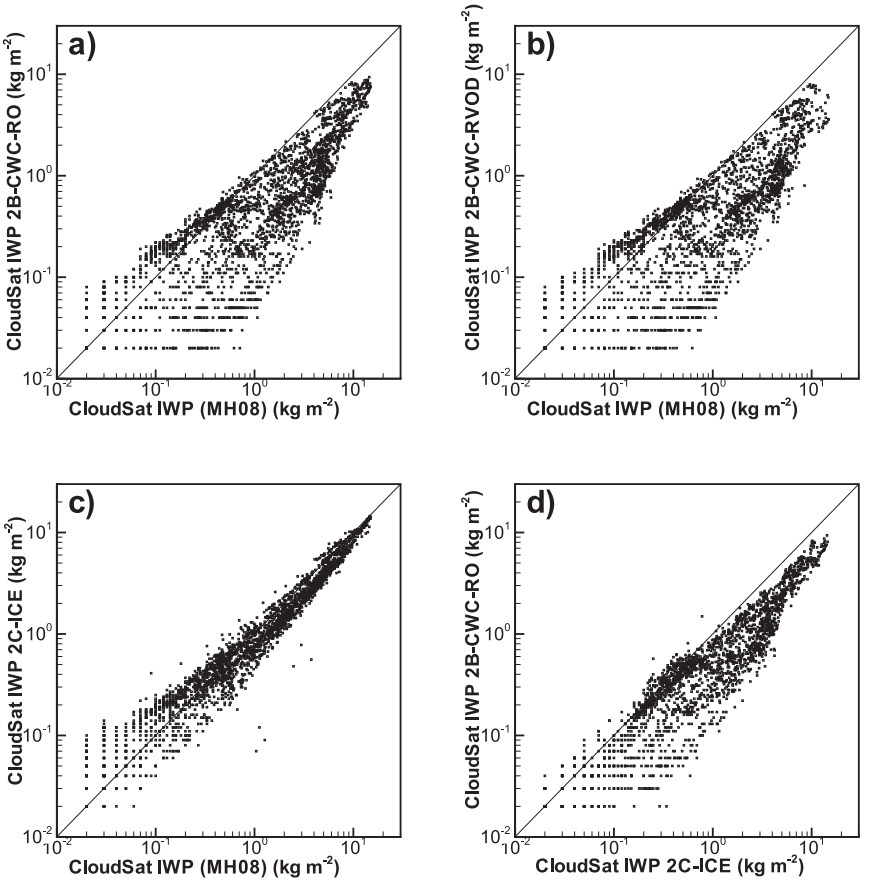

FIG. 6. Scatterplots of different IWP retrievals for 12 observational stratiform precipitation events: (a) 2B-CWC-RO vs MH08, (b) 2B-CWC-RVOD vs MH08, (c) 2C-ICE vs MH08, and (d) 2B-CWC-RO vs 2C-ICE.

intercomparisons provided some mixed results. While Delanoe et al. (2013) found that the standard *CloudSat* IWC products were often larger than the DARDAR retrievals, Deng et al. (2013) data suggest that the 2C-ICE and DARDAR IWC values were on average larger (by 10%–50%) than those from the 2B-CWC-RVOD product. Protat et al. (2010) reported that statistical intercomparisons of spaceborne and ground-based retrievals in the vicinity of a cloud radar site in Darwin indicated larger 2B-CWC-RVOD IWC values at heights less than 10 km as compared to the values inferred from surface-based sensors. Mace (2010) mentions that *CloudSat* IWC retrievals were biased by about 18% low compared to in situ measurements collected from several aircraft underflights in the vicinity of Costa Rica. It should be pointed out, however, that the previous IWC intercomparisons mentioned above considered general ice cloud events. A fraction of nonprecipitating clouds in those events is expected to be very significant (if not dominant).

b. *Intercomparisons of* CloudSat *and WSR-88D IWP retrievals*

Intercomparisons of *CloudSat* measurements with ground-based radar or model data have been previously performed for different applications (e.g., Hudak et al.

TABLE 1. Statistical scores characterizing comparisons of different *CloudSat* IWP retrievals. IWP units are kilograms per meter squared.

	Mean IWP_y	Mean IWP_x	Correlation r	RMB	NMAD	No. of data points
2B-CWC-RO vs MH08	0.96	2.21	0.90	−56%	61%	2972
2B-CWC-RVOD vs MH08	0.72	1.81	0.83	−59%	63%	2643
2C-ICE vs MH08	1.74	2.04	0.98	−14%	20%	2917
2B-CWC-RO vs 2C-ICE	0.88	1.75	0.93	−51%	54%	2658

2008; Woods et al. 2008; Turk et al. 2011; Matrosov 2014). Here IWP retrieval results obtained when observing mostly stratiform precipitating systems are compared. For all 12 observational events, Fig. 7a depicts a scatterplot of the IWP values from collocated vertical profiles retrieved from *CloudSat* and from the WSR-88D measurements using the approaches described in the previous section. For a better temporal collocation of the comparison data, the WSR-88D-based IWP values were obtained by the linear interpolation of results from two consecutive volume scans that bracket the exact time of the *CloudSat* retrievals. The comparisons are shown with respect to the *CloudSat* MH08 IWP values, which are (as shown in the previous subsection) in relatively good agreement with the 2C-ICE IWP retrievals.

The IWP data corresponding to the *CloudSat* profiles, which were completely or partially in the WSR-88D cone of silence, were excluded from the comparisons. Excluded also were the data corresponding to the radar distances, for which the WSR-88D completely or partially overshot the ice hydrometeor layer, that is, when the lower edge of the lowest WSR-88D beam was higher than the freezing-level altitude [$h_1^{(l)} < h_{fl}$]. These exclusions resulted in fewer data points available for ground-based and satellite comparisons compared to those in Fig. 6 where intercomparisons of different *CloudSat* IWP products are shown. It also resulted in relatively higher IWP values retained in Fig. 7 in comparison with the ones in Fig. 6. This is explained by the fact that many lower IWP data points present in Fig. 6 corresponded to the *CloudSat* measurements at greater distances from the ground radar sites when the WSR-88D overshooting was frequent.

The statistical metric scores of the retrievals derived from the WSR-88D and *CloudSat* measurements are shown in Table 2. An overall agreement between ground-based and satellite-derived IWP values is relatively good. The correlation coefficient is relatively high (0.7) and the mean bias is rather low (13%). The NMAD value of 55% is on the order of the uncertainty of estimating ice content from radar reflectivity measurements (e.g., MH08). The use of the 2C-ICE IWP retrievals instead of the MH08 IWP retrievals for comparisons with WSR-88D-based IWP estimates (the corresponding graphs are not shown) results in the RMB increase to 25% and in a rather modest change in the NMAD (~56%). 2B-CWC-RO IWP retrievals, however, are biased low by 50%–60% compared the other two (i.e., 2C-ICE and MH08) *CloudSat* retrievals and WSR-88D-based IWP estimates.

Since the resolution of the WSR-88D reflectivity measurements changes with distance from the ground-based radar, it is instructive to assess if this distance

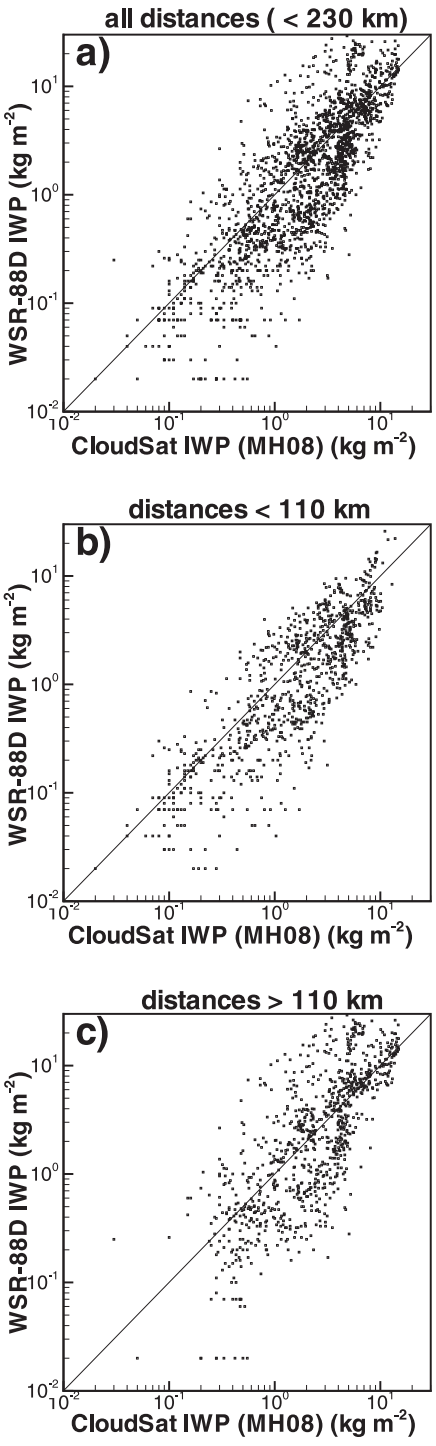

FIG. 7. Scatterplots of IWP retrieved from *CloudSat* measurements (MH08) vs WSR-88 matched estimates: (a) for all ranges from the WSR-88D sites, (b) for WSR-88D ranges < 110 km, and (c) for WSR-88D ranges > 110 km. Data points for profiles, which are totally or partially in the cone of silence and for which WSR-88D measurements partially or totally overshot the ice hydrometeor layers, were excluded.

TABLE 2. Statistical scores characterizing comparisons of WSR-88D and *CloudSat* MH08 IWP retrievals for different WSR-88D distances D. IWP units are kilograms per meter squared.

	Mean IWP WSR-88D	Mean IWP *CloudSat*	Correlation r	RMB	NMAD	No. of data points
$D < 230$ km	3.61	3.18	0.70	13%	55%	1838
$D < 110$ km	2.46	2.70	0.74	−9%	57%	908
110 km $\leq D < 230$ km	4.28	3.58	0.68	19%	54%	930

affects the satellite and ground-based radar IWP retrieval comparisons in a significant way. More than half of the total number of data point comparisons in Fig. 7a correspond to relatively short distances from ground-based radar sites (<110 km). The IWP comparisons for these distances are shown in Fig. 7b. Figure 7c depicts the comparisons for longer distances. The corresponding statistical scores are given in Table 2. It can be seen from the presented data that the NMAD values depending on distance change rather little. The change in the RMB values, while being more pronounced, is still within retrieval uncertainties. Given these uncertainties and overall data scatter, it can be suggested that the presented data do not indicate strong distance-dependent biases of WSR-88D IWP retrievals within ranges of the level-II NEXRAD products (i.e., for ranges less than 230 km).

6. Summary and conclusions

This study suggests an approach to retrieve the total ice content in a vertical atmospheric column (i.e., the ice water path) of precipitating systems using operational WSR-88D measurements obtained with standard precipitation VCPs. The results of this study show that IWP information can be deduced from these measurements at least in predominantly stratiform precipitation systems producing rain in the lower atmospheric layers. Such systems are typically characterized by the radar bright band, which effectively separates the precipitating ice cloud regions from liquid hydrometeor layer containing rain. IWP values are obtained by vertically integrating WSR-88D reflectivity-based IWC estimates in the ice-phase-dominated layers located above the freezing level. Oversampling and/or gaps resulting from a particular VCP used for WSR-88D volume scanning are accounted for when calculating these IWP values.

Although other vertically integrated functions of observed WSR-88D reflectivity, such as the vertically integrated liquid (VIL), have been used previously for identifying hazardous weather events (e.g., Amburn and Wolf 1996), they did not provide the phase separation and mostly were aimed at identifying the severity of precipitation (e.g., serving as an indicator of hail size). IWP is an important cloud parameter that is used in many model applications. It is routinely retrieved from both spaceborne and ground-based dedicated cloud radar measurements (e.g., Stephens et al. 2008). The combined IWP and standard rain-rate retrievals from operational WSR-88D measurements can provide useful information on rain formation processes especially in stratiform precipitating systems where ice/snow particle melting aloft is the main mechanism of raindrop formation.

The WSR-88D IWP estimates were evaluated using the spaceborne W-band radar-based *CloudSat* IWP retrievals for 12 experimental events observed during the period 2006–12 when the satellite passed over vicinities of the KGWX and KSHV radar sites. Although these events were mostly stratiform they also contained small areas of convective rainfall. The standard *CloudSat* products as well as IWP values from the method developed specifically for thick ice clouds with accounting for ice hydrometers nonsphericity (MH08) were used for comparisons with WSR-88D retrievals. The *CloudSat* 2C-ICE and MH08 IWP values were in rather close agreement, while the *CloudSat* standard 2B-CWC-RO product (and its 2B-CWC-RVOD modification) provided IWP values, which were generally smaller by about 50% relative to the other two *CloudSat* estimates if the whole range of IWP changes is considered. The differences between results from the standard products and 2C-ICE and MH08 IWP values were, however, typically smaller for lower IWP values.

Comparisons of the WSR-88D-derived IWP with closely collocated in space and time *CloudSat*-based estimates of this parameter from the MH08 and 2C-ICE methods indicated relatively high correlation between ground-based and spaceborne IWP retrievals with the correlation coefficient being around 0.7. The WSR-88D retrievals were somewhat higher on average (by ~15%–25%) than *CloudSat* retrievals. The relative mean differences between satellite and ground-based IWP estimates were around 50%–60%, which is on the order of ice content retrieval uncertainties using the radar reflectivity measurements. Although the vertical resolution of WSR-88D measurements degrades with distance

from a ground-based radar because of beam broadening effects, results of comparisons between ground-based and satellites retrievals of IWP exhibited relatively little distance dependence.

Overall the agreement between experimentally derived IWP values using WSR-88D measurements conducted with standard VCPs and products from existing satellite radar techniques is encouraging. It suggests that, despite resolution limitations, operational NEXRAD measurements employing standard scanning procedures can be used for quantitative estimation of IWP in stratiform precipitating cloud systems with uncertainties similar to those inherent to satellite radar techniques. Since there are more than 150 NEXRAD units in the United States, precipitating ice content retrievals from WSR-88D measurements might present valuable cloud information on large spatial scales. More quantitative intercomparisons involving different ground-based radar localities will be needed in the future to better understand the retrieval uncertainties.

The recent polarimetric upgrade of WSR-88D systems provides additional opportunities for future enhancements of cloud parameter retrievals using the NEXRAD network radars. These enhancements are potentially associated with further developments and validations of polarimetric methods for ice content retrievals that use measurements of differential reflectivity and phase (e.g., Ryzhkov et al. 1998). Traditional reflectivity-based ice content retrieval techniques can also be refined by tuning their coefficients for the use with different type particle populations (e.g., aggregates versus more pristine crystal shapes), which can be identified using polarimetric radar approaches (e.g., Ryzhkov et al. 2005).

Future research will also include investigating possibilities for the use of WSR-88D and *CloudSat* dual-frequency ratio (DFR) measurements. Such synergetic use of collocated ground-based and satellite measurements could provide robust information on characteristic sizes of ice hydrometeors using DFR–characteristic size relations that are relatively immune to variability of particle density (e.g., Matrosov 1998), thus providing an additional constraint for ice-cloud-property retrievals.

Acknowledgments. This study was funded in part by the NASA project NNX13AQ31G and the NOAA Hydrometeorology Testbed project.

REFERENCES

Amburn, S., and P. Wolf, 1996: VIL density as a hail indicator. Preprints, *18th Conf. on Severe Local Storms,* San Francisco, CA, Amer. Meteor. Soc., 581–585.

Austin, R., A. J. Heymsfield, and G. L. Stephens, 2009: Retrieval of ice cloud microphysical parameters using the *CloudSat* millimeter-wave radar and temperature. *J. Geophys. Res.,* **114,** D00A23, doi:10.1029/2008JD010049.

Bringi, V. N., and V. Chandrasekar, 2001: *Polarimetric Doppler Weather Radar.* Cambridge University Press, 636 pp.

Delanoe, J., A. Protat, O. Jourdan, J. Pelon, M. Papazzoni, R. Dupuy, J.-F. Gayet, and C. Jouan, 2013: Comparisons of airborne in situ, airborne radar–lidar, and spaceborne radar–lidar retrievals of polar ice cloud properties sampled during the POLARCAT campaign. *J. Atmos. Oceanic Technol.,* **30,** 57–73, doi:10.1175/JTECH-D-11-00200.1.

Deng, M., G. G. Mace, Z. Wang, and R. P. Lawson, 2013: Evaluation of several A-Train ice cloud retrieval products with in situ measurements collected during the SPARTICUS campaign. *J. Appl. Meteor. Climatol.,* **52,** 1014–1030, doi:10.1175/JAMC-D-12-054.1.

Doviak, R. J., and D. S. Zrnic, 1993: *Doppler Radar and Weather Observations.* Academic Press, 562 pp.

Hogan, R. J., and C. D. Westbrook, 2014: Equation for the microwave backscatter cross section of aggregate snowflakes using self-similar Rayleigh–Gans approximation. *J. Atmos. Sci.,* **71,** 3292–3301, doi:10.1175/JAS-D-13-0347.1.

——, M. P. Mittermaier, and A. J. Illingworth, 2006: The retrievals of ice water content from radar reflectivity factor and temperature and its use in evaluating a mesoscale model. *J. Appl. Meteor. Climatol.,* **45,** 301–317, doi:10.1175/JAM2340.1.

Houze, R. A., 1997: Stratiform precipitation in regions of convection: A meteorological paradox. *Bull. Amer. Meteor. Soc.,* **78,** 2179–2196, doi:10.1175/1520-0477(1997)078<2179:SPIROC>2.0.CO;2.

Hudak, D., P. Rodrigez, and N. Donaldson, 2008: Validation of the *CloudSat* precipitation occurrence algorithm using Canadian C band radar network. *J. Geophys. Res.,* **113,** D00A07, doi:10.1029/2008JD009992.

Kirstetter, P. E., H. Andrieu, B. Boudevillain, and G. Delrieu, 2013: A physically based identification of vertical profiles of reflectivity from volume scan radar data. *J. Appl. Meteor. Climatol.,* **52,** 1645–1663, doi:10.1175/JAMC-D-12-0228.1.

Mace, G. G., 2010: Cloud properties and radiative forcing over the maritime storm tracks of the Southern Ocean and North Atlantic derived from A-Train. *J. Geophys. Res.,* **115,** D10201, doi:10.1029/2009JD012517.

Matrosov, S. Y., 1997: Variability of microphysical parameters in high-altitude ice clouds: Results of the remote sensing method. *J. Appl. Meteor.,* **36,** 633–648, doi:10.1175/1520-0450-36.6.633.

——, 1998: A dual-wavelength radar method to measure snowfall rate. *J. Appl. Meteor.,* **37,** 1510–1521, doi:10.1175/1520-0450(1998)037<1510:ADWRMT>2.0.CO;2.

——, 2007: Potential for attenuation-based estimations of rainfall rate from *CloudSat*. *Geophys. Res. Lett.,* **34,** L05817, doi:10.1029/2006GL029161.

——, 2008: Assessment of radar signal attenuation caused by the melting hydrometeor layer. *IEEE Trans. Geosci. Remote Sens.,* **46,** 1039–1047, doi:10.1109/TGRS.2008.915757.

——, 2014: Intercomparisons of *CloudSat* and ground-based radar retrievals of rain rate over land. *J. Appl. Meteor. Climatol.,* **53,** 2360–2370, doi:10.1175/JAMC-D-14-0055.1.

——, and A. J. Heymsfield, 2008: Estimating ice content and extinction in precipitating cloud systems from *CloudSat* radar measurements. *J. Geophys. Res.,* **113,** D00A05, doi:10.1029/2007JD009633.

——, and A. Battaglia, 2009: Influence of multiple scattering on *CloudSat* measurements in snow: A model study. *Geophys. Res. Lett.,* **36,** L12806, doi:10.1029/2009GL038704.

——, F. M. Ralph, P. J. Neiman, and A. B. White, 2014: Quantitative assessment of operational weather radar rainfall estimates over California's northern Sonoma County using HMT-West data. *J. Hydrometeor.,* **15,** 393–410, doi:10.1175/JHM-D-13-045.1.

Melnikov, V. M., D. S. Zrnic, R. J. Doviak, P. B. Chilson, D. B. Mechem, and Y. L. Kogan, 2011: Prospects of the WSR-88D radar for cloud studies. *J. Appl. Meteor. Climatol.,* **50,** 859–872, doi:10.1175/2010JAMC2303.1.

Protat, A., J. Delanoe, E. J. O'Connor, and T. S. L'Ecuyer, 2010: The evaluation of *CloudSat* and *CALIPSO* ice microphysical products using ground-based cloud radar and lidar observations. *J. Atmos. Oceanic Technol.,* **27,** 793–810, doi:10.1175/2009JTECHA1397.1.

Ryzhkov, A. V., D. S. Zrnic, and B. A. Gordon, 1998: Polarimetric method for ice water determination. *J. Appl. Meteor.,* **37,** 125–134, doi:10.1175/1520-0450(1998)037<0125:PMFIWC>2.0.CO;2.

——, S. E. Giangrande, and T. J. Schuur, 2005: Rainfall estimation with a polarimetric prototype of WSR-88D. *J. Appl. Meteor.,* **44,** 502–515, doi:10.1175/JAM2213.1.

Sassen, K., S. Matrosov, and J. Campbell, 2007: *CloudSat* spaceborne 94 GHz radar bright bands in the melting layer: An attenuation-driven upside-down lidar analog. *Geophys. Res. Lett.,* **34,** L16818, doi:10.1029/2007GL030291.

Stephens, G. L., and Coauthors, 2008: *CloudSat* mission: Performance and early science after the first year of operation. *J. Geophys. Res.,* **113,** D00A18, doi:10.1029/2008JD009982.

Tanelli, S., S. L. Durden, E. Im, K. S. Pak, D. G. Reinke, P. Partain, J. M. Haynes, and R. Marchand, 2008: *CloudSat*'s cloud profiling radar after two years in orbit: Performance, calibration, and processing. *IEEE Trans. Geosci. Remote Sens.,* **46,** 3560–3573, doi:10.1109/TGRS.2008.2002030.

Turk, F. J., K. W. Park, Z. S. Haddad, P. Rodriguez, and D. R. Hudak, 2011: Constraining *CloudSat*-based snowfall profiles using surface observations and C-band ground radar. *J. Geophys. Res.,* **116,** D23205, doi:10.1029/2011JD016126.

Woods, C. P., D. E. Waliser, J.-L. Li, R. T. Austin, G. L. Stephens, and D. G. Vane, 2008: Evaluating *CloudSat* ice water content retrievals using a cloud-resolving model: Sensitivities to frozen particle properties. *J. Geophys. Res.,* **113,** D00A11, doi:10.1029/2008JD009941.

Zhang, J., and Coauthors, 2011: National Mosaic and Multi-Sensor QPE (NMQ) system: Description, results, and future plans. *Bull. Amer. Meteor. Soc.,* **92,** 1321–1338, doi:10.1175/2011BAMS-D-11-00047.1.